2018 European Control Conference (ECC)
June 12-15, 2018. Limassol, Cyprus

Reconfiguration control of in-wheel electric vehicle based on battery state of charge

András Mihály and Péter Gáspár

Abstract— **The paper deals with reconfiguration control of electric vehicles operated by in-wheel motors and steer-by-wire steering system. The control reconfiguration is based on a power management method considering battery state of charge (SOC). In case the condition of the battery is critical and the vehicle is traveling on a slope, a high level reconfiguration is applied preferring yaw moment generation over steering actuation, by which energy recuperation can be improved and battery state of charge can be enhanced. The proposed control reconfiguration is implemented based on Linear Parameter Varying (LPV) framework, where a monitoring signal related to battery SOC scales the actuator selection. The operation of the presented power management method based on control reconfiguration is demonstrated in CarSim simulation environment.**

I. Introduction

One of the most challenging tasks in electric vehicle design is to enhance the range of the vehicle. Apart from the relatively smaller range compared to conventional vehicles, other motivations for range extension are related to the fact that the charging of the batteries is time consuming and the infrastructure is less developed. For this reason, researchers and industrial companies have been focusing on improving the batteries as one of the key elements of electric vehicles. Also, the use of supplementary energy sources such as solar panels is becoming widespread, and the recuperation of the vehicle motion energy has also been investigated broadly, see [1], [2].

The advantages provided by in-wheel motor driven electric vehicles are broad, since such architecture not only enables to design more effective vehicle dynamic controllers as proposed by [3], [4], [5], but also gives an opportunity to enhance energy optimality of the electric vehicles, see [6], [7]. As the operation of the hub motors can be controlled and monitored more precisely and faster compared to conventional electric drive trains, regenerative braking can be realized more efficiently, see [8], [9].

Present paper deals with the trajectory tracking control of a four-wheel independently-actuated (4WIA) electric vehicle, with considering battery SOC in the actuator selection. The main novelty of the proposed method lies in the reconfiguration design, by which the cornering resistance energy originating from steering intervention can be substituted with regenerative braking applied independently on the wheels of the 4WIA vehicle. By this mean, battery SOC can be enhanced, also effecting positively the range of the electric vehicle.

The paper is organized as follows: Section II describes the bicycle model used for control design. Section III presents the proposed reconfiguration design considering battery SOC using LPV control methods. Section IV deals with the control architecture and the distribution of the high-level signals among the low-level actuators. Section V validates the effectiveness of the proposed method in CarSim simulation environment. Finally, some conclusive statements are listed in Section VI.

II. Vehicle model for trajectory tracking

For the modeling of the in-wheel electric vehicle planar motion, the two-track bicycle model is utilized, as depicted in Figure 1. Hence, the following differential equations are given as follows:

$$J\ddot{\psi} = c_1 l_1 \alpha_1 - c_2 l_2 \alpha_2 + M_z \tag{1a}$$

$$m\dot{\xi}(\dot{\psi} + \dot{\beta}) = c_1\alpha_1 + c_2\alpha_2 \tag{1b}$$

$$m\ddot{\xi} = F_l - F_d \tag{1c}$$

where m is the vehicle total mass, J stands for the yaw inertia, c_1 and c_2 are lateral tire stiffness of the wheels on the front and rear axles assumed to be identified. Note that l_1 and l_2 are geometrical parameters of the 4WIA vehicle. The front and rear wheels side slip angles are given as $\alpha_1 = \delta - \beta - \dot{\psi} l_1/\dot{\xi}$ and $\alpha_2 = -\beta + \dot{\psi} l_2/\dot{\xi}$, β is the vehicle side-slip angle, ξ stands for the longitudinal displacement, while $\dot{\psi}$ represents the yaw rate of the 4WIA vehicle.

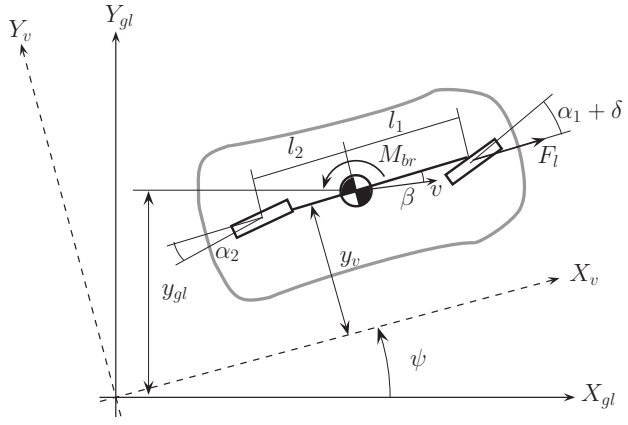

Fig. 1. Single track bicycle model

There are three high-level control inputs defined: F_l is the longitudinal force, M_z is the yaw moment realized by the

A. Mihály and P. Gáspár are with Institute for Computer Science and Control, Hungarian Academy of Sciences, Hungary. E-mail: [andras.mihaly;peter.gaspar]@sztaki.mta.hu

This work has been supported by the GINOP-2.3.2-15-2016-00002 grant of the Ministry of National Economy of Hungary and by the European Commission through the H2020 project EPIC under grant No. 739592.

independent torque generation of the hub motors, while δ is the steering angle of the front wheels.

In equation (1) the longitudinal disturbance force F_d consists the aerodynamic drag, the road slope and rolling resistance of the vehicle. Hence, it can be modeled with the following nonlinear equation: $F_d = 0.5C_d\rho A_F\dot{\xi}^2 + mg\sin\alpha_s + mgf\cos\alpha_s$, where C_d stands for the drag coefficient, ρ represents air mass density, A_F is the frontal surface, α_s is the road slope angle, f is the road friction coefficient and g is the gravitational constant.

As the differential equations described in (1) are nonlinear due to the velocity of the vehicle, it is chosen as scheduling variables $\rho_1 = \dot{\xi} \in [5m/s, 35m/s]$. Also, $\rho_2 = \frac{1}{\xi}$ and $\rho_3 = \frac{1}{\dot{\xi}^2}$ are selected as scheduling variables. Denoting $\rho = \begin{bmatrix}\rho_1 & \rho_2 & \rho_3\end{bmatrix}^T$, the nonlinear model can be transformed into an LPV model with the following state-space representation:

$$\dot{x} = A(\rho)x + B_1 w + B_2(\rho)u, \tag{2}$$

where $x = \begin{bmatrix}\dot{\xi} & \xi & \dot{\psi} & \beta\end{bmatrix}^T$ is the state vector, $u = \begin{bmatrix}F_l & \delta & M_z\end{bmatrix}^T$ is the input vector, $y = \begin{bmatrix}\dot{\xi} & \dot{\psi}\end{bmatrix}^T$ is the output vector and $w = \begin{bmatrix}F_d\end{bmatrix}^T$ vector contains the disturbances of the system.

III. Reconfiguration control considering battery SOC

The gain scheduling LPV control design is based on the nonlinear bicycle model equations defined by (1). The goal of the control design is to realize both velocity and road trajectory tracking for the 4WIA electric vehicle. Yaw-rate tracking control has been studied by several authors for both conventional and in-wheel electric vehicles, see [10], [11], [12]. In order to ensure velocity and road trajectory tracking, appropriate reference signals must be selected. Since it is assumed that the driver follows the road curvature with applying steering input δ_d, the reference yaw-rate can be defined as follows: $\dot{\psi}_{ref} = \dot{\xi}/d \cdot e^{-\frac{t}{\tau}} \cdot \delta_d$ where d is a function of the velocity, understeer gradient and the geometric parameters of the vehicle, while τ is a time constant, see [13]. As for the longitudinal control, the driver of the 4WIA vehicle sets a desired velocity, thus $\dot{\xi}_{ref}$ is also defined as a reference signal. Next, a reference vector $R = [\dot{\xi}_{ref}\ \dot{\psi}_{ref}]^T$ is constructed containing both reference signals in the planar plane.

As the aim of the controller design is to guarantee tracking of the reference signals formulated in vector R, two optimization criterion is given for this purpose. First, the velocity error between the reference signal given by the driver and the actual vehicle velocity must be minimized by satisfying the optimization criterion : $z_{\dot{\xi}} \to 0$. Next, the yaw rate error between the driver defined reference and the actual vehicle yaw rate measured with widespread gyroscope sensor must be minimized, thus a second optimization criterion $z_{\dot{\psi}} \to 0$ is formulated. The two performances defined are then put in a performance vector $z_1 = \begin{bmatrix}z_\xi & z_{\dot{\psi}}\end{bmatrix}^T$. Finally, in order to avoid actuator saturation, construction limits of the steer-by-wire steering system and the electric hub motors must also be considered, thus a second performance vector is given for the control inputs as $z_2 = \begin{bmatrix}F_l & \delta & M_z\end{bmatrix}^T$.

A. High-level controller design

The gain scheduling LPV control is based on the closed-loop interconnection architecture depicted in Figure 2. Here, the different control objectives are defined with weighting functions corresponding to the given control goal. Although these weighting functions are given in frequency domain, their state-space representation are used in the control design.

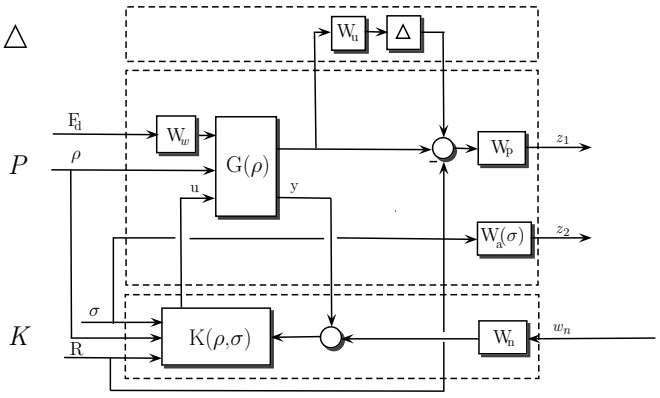

Fig. 2. Closed-loop interconnection structure

Weighting function W_p represents a trade-off among control performances defined in performance vector z_1. Hence, two weighting function has been designed for velocity and yaw rate tracking in a second-order proportional form. These function can be considered as penalty functions, i.e weights are large where small signals are desired and vice verse. Weighting functions noted with W_w and W_n describe disturbance and sensor noises, while unmodeled dynamics of the 4WIA vehicle are represented with weighting function W_u.

One of the main objective in the high-level controller design is to achieve reconfiguration between actuators considering battery SOC, as detailed in Section III-B. Hence, with appropriately design of the weighting functions noted with W_a in Figure 2, the split among steering and torque vectoring can be changed corresponding to the vehicle state. Hence, a weighting function for the steering angle input $W_{a\delta} = (\delta_{max}\chi_1)/(\sigma)$ and for the yaw moment input $W_{aMz} = (\sigma)/(M_{zmax}\chi_2)$ is given, where χ_1 and χ_2 are design parameters selected to realize control redistribution, δ_{max} is the maximum value of the steering angle, M_{zmax} is the maximum yaw moment, while $\sigma \in [0.01, 1]$ is a the monitoring variable representing the balance among steering intervention and and yaw moment generation. Hence, selecting $\sigma = 1$ only steering is applied during a cornering maneuver, while in case of choosing $\sigma = 0.01$ only differential torque is generated by the in-wheel motors of the 4WIA vehicle.

The LPV performance problem described in [14],is to design a parameter-varying controller in a manner, that

quadratic stability of the closed-loop system can be achieved while the induced $\mathcal{L}_2$ norm from the disturbance ω to the performances z is smaller than γ. Hence, above minimization problem can be written as follows:

$$\inf_{K} \sup_{\rho \in \mathcal{F}_\mathcal{P}} \sup_{\|w\|_2 \neq 0, w \in \mathcal{L}_2} \frac{\|z\|_2}{\|w\|_2} \leq \gamma. \tag{3}$$

The solution of the quadratic LPV γ-performance problem is governed by the set of infinite dimensional LMIs being satisfied for all $\rho \in \mathcal{F}_\mathcal{P}$. This can be solved numerically, since it is a convex problem. In practice, the parameter space is gridded and the set of LMIs are solved on the subset of $\mathcal{F}_\mathcal{P}$. Finally, the state space representation of the designed controller $K(\rho)$ $\rho \in \mathcal{F}_\mathcal{P}$ is given, see [15].

B. Consideration of battery SOC

The proposed reconfiguration method is based on the estimation of battery SOC. Several wide spread battery models can be found in the literature, including detailed models containing chemical reactions and simplified equivalent circuit and polynomial models. In [16] and [17] detailed models are given for NiMH batteries. In [16] the detailed chemical reactions are collected in a state space model for NiMH batteries. In [17] a detailed algorithm for the estimation of NiMH battery SOC can be found, which method can also be adapted for lead-acid and Li-ion batteries as well.

In the paper a model presented in [18] is considered, which represents the operation of a lithium-ion battery pack. Assuming the battery to consist N_B number of cells all equalized providing the requested electrical power P_B, the differential equation for battery SOC can be given for a single cell as follows:

$$\frac{dSOC}{dt} = -\frac{V_0(SOC) - \sqrt{V_0(SOC)^2 - 4R_{in}\frac{P_B}{N_B}}}{2R_{in}Q_{max}} \tag{4}$$

where V_0 is the open circuit voltage, R_{in} is the internal resistance and Q_{max} is the maximum battery cell charge. Note, that in equation (4) the requested power P_B can be calculated as

$$P_B = N_B P_C = N_B(V_0 I_C - R_{in} I_C^2)$$

where I_C is the instantaneous battery current.

A brushless DC electric motor model was also developed for all four wheels of the 4WIA vehicle and connected to the battery model described above. The block has been constructed such way, that it can handle both positive and negative torque request T. Hence, the electrical motor current I can be given as follows:

$$I = \frac{T\omega}{V} \begin{cases} I_{dis}, & \text{if } T > 0 \\ I_{chg}, & \text{if } T < 0 \end{cases} \tag{5}$$

where ω is the angular velocity and V is the battery voltage connected to the value of the battery SOC, I_{dis} is the battery discharging current, I_{chg} is the battery charging current. Thus, in case of a negative torque request given by the torque allocation method listed in Section IV, the motor model generates a charging current for the battery model.

Next, assuming the road slope angle λ to be measured as proposed by several authors [19], [20], a decision logic has been designed to determine the actuator scaling parameter σ considering the possibility to recuperate maximal energy when traveling on a slope. In case the vehicle is traveling on uphill road section, i.e $\lambda > 0$, steering intervention is applied ($\sigma = 1$) regardless of the battery SOC. On the other hand, in case the vehicle is traveling on a slope ($\lambda < 0$) and the battery SOC has already reached a predefined value (80 %), the high-level controller is reconfigured ($\sigma = 0.01$) to use differential braking instead of steering intervention. Hence, the actuator scaling decision logic can be written as follows:

$$\sigma = \begin{cases} 1, & \text{if } SOC > 80\% \\ 1, & \text{if } SOC < 80\% \text{ and } \lambda > 0 \\ 0.01, & \text{if } SOC < 80\% \text{ and } \lambda < 0 \end{cases} \tag{6}$$

IV. Architecture of the reconfiguration control

The presented reconfiguration method considering battery SOC is implemented in a multi-layer structure, with the architecture depicted in Figure 3.

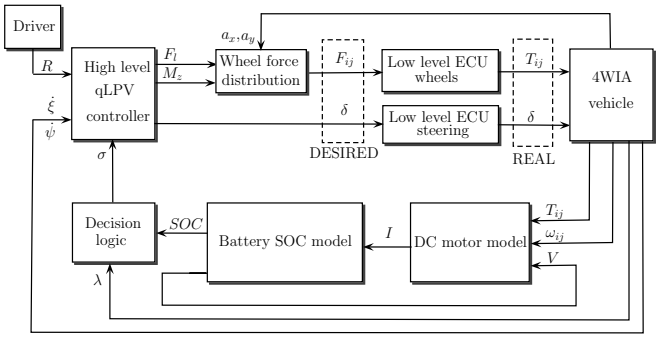

Fig. 3. Structure of the control system

The first layer contains the high-level LPV controller, which calculates the control signals based on the driver reference inputs, the measured vehicle velocity and the value of the actuator scaling scheduling variable σ.

The second layer is responsible for the allocation of the high-level control signals, i.e the longitudinal force, yaw moment and steering angle. The applied distribution method considering vehicle dynamical and stability aspects has already been presented in [21], thus here only a brief description is given. By assuming small steering angles and knowing the vehicle geometrical parameters, load distribution between the front and rear axles are formulated as follows:

$$\frac{F_{zf}}{F_{zr}} = \frac{mgl_2 - ma_x h_{COG}}{mgl_1 + ma_x h_{COG}} = \kappa \tag{7}$$

where h_{COG} is the height of the gravity center. Since the sum of the applied wheel forces must equal to that prescribed by the high-level controller, the following equation must hold:

$$F_l = F_{fL} + F_{fR} + F_{rL} + F_{rR} \tag{8}$$

where F_{ij} $i \in [f = front, r = rear]$, $j \in [L = left, R = right]$ represents longitudinal wheel forces. Yaw moment M_z calculated by the high-level LPV controller must also be realized, thus the following constraint must also hold:

$$M_z = (-F_{fL} + F_{fR})\frac{b_f}{2} - (F_{rL} + F_{rR})\frac{b_r}{2} \tag{9}$$

Rearranging above equations, the desired longitudinal wheel forces can be expressed as follows:

$$\begin{aligned} F_{fL} &= \frac{F_l}{2\left(1+\frac{1}{\kappa}\right)} - \frac{M_z}{b_f + \frac{1}{\kappa}b_r}, \quad F_{rL} = \left(\frac{1}{\kappa}\right)F_{fL}, \\ F_{fR} &= \frac{F_l}{2\left(1+\frac{1}{\kappa}\right)} + \frac{M_z}{b_f + \frac{1}{\kappa}b_r}, \quad F_{rR} = \left(\frac{1}{\kappa}\right)F_{fR} \end{aligned} \tag{10}$$

Finally, the hub motor torques designed for the 4WIA electric vehicle can be written as $T_{ij} = R_{eff}F_{ij}$, where R_{eff} is the effective rolling radius of the wheels.

The third layer models the operation of the low-level controllers, i.e it represents the tracking of the distributed electric motor torques and the prescribed steering angle. Here, dynamics of the steer-by-wire steering system is modeled as a first-order system as proposed in [22]. The current control of the in-wheel hub motors are simplified in this layer as proposed in [23], thus the following equation describes the relation between the prescribed wheel torque and the generated torque:

$$T_{motor}(s) = \frac{T(s)(1+\eta)}{1 + 2\zeta + 2\zeta^2} \tag{11}$$

where T_{motor} is the electric motor torque, T is the prescribed torque, while ζ and η represents the dynamic response and steady state error of the electric hub motors.

Finally, the fourth layer depicted in Figure 3 is responsible for modeling the operation of the electric in-wheel motors and the lithium-ion battery pack. These models detailed in Section III-B serves to calculate the battery SOC and the corresponding monitoring variable σ determined by equation (6).

V. Simulation Results

The selected vehicle for the simulation is a small 4WIA vehicle, with the main physical and dynamic parameters listed in Table I, while the electric in-wheel motor parameters are depicted in Table II. The selected road for the simulation contains two curves as depicted in Figure 4(a), where the first curve is located on the uphill section, while the second curve is located on the downhill road section, see Figure 4(b). The reference velocity of the vehicle is set to constant $54\ km/h$, while the reference yaw rate for the vehicle given by the driver is shown in Figure 4(c).

Note that several vehicle dynamic signals can be measured in real vehicles using widespread wheel speed sensors and a gyroscopes, thus vehicle velocity, yaw rate, longitudinal and lateral accelerations are also measured in CarSim. Also, steering angle δ is assumed to be measured by steering angle sensor. The goal of the simulation is to compare the results of the conventional trajectory control method and the

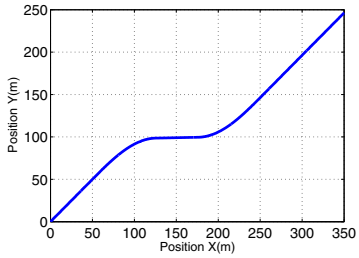

(a) Racetrack X-Y plane

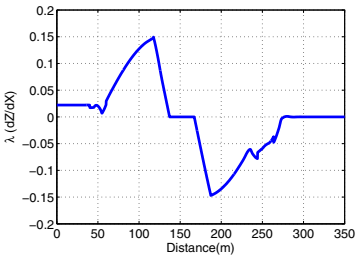

(b) Road slope

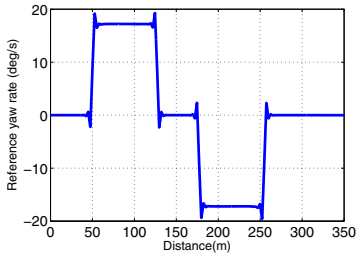

(c) Reference yaw rate

Fig. 4. Road and driver references

TABLE I

Parameters of the 4WIA vehicle

Parameter	Value	Unit
Vehicle mass (m)	830	kg
Yaw moment of inertia (J)	1110.9	kgm^2
Distance from C.G to front axle (l_1)	1.103	m
Distance from C.G to rear axle (l_2)	1.244	m
Tread front (b_f)	1.416	m
Tread rear (b_r)	1.375	m
Height of COG (h_{COG})	0.54	m
Cornering stiffness front (c_1)	22	kN/rad
Cornering stiffness rear (c_2)	85	kN/rad
Aerodynamic drag co-efficient (c_w)	0.343	$-$
Front contact surface (A)	1.6	m^2

TABLE II

Hub motor parameters

Parameter	Value	Unit
Total motor mass	32.15	kg
Output power	6	kW
Peak output torque	577	Nm
Continuous output torque	300	Nm
Terminal voltage	100	V
Continuous Current	322	A
Peak Current	550	A
Line-Line Resistance	0.16	Ohm
Back EMF Constant	110	$V/kRPM$
Torque Constant	1.05	Nm/A
Armature Inductance	11	mH

battery SOC based reconfiguration method presented in the paper. Thus, two simulation has been performed with similar settings: in the first simulation the cornering maneuver is performed solely using steering intervention, while in the second simulation the control is reconfigured preferring yaw moment generation.

The scheduling and monitoring variables of the LPV controller is depicted in Figure 5. It is well demonstrated, that while scheduling variable ρ_1 describing the velocity of the 4WIA vehicle is similar for both cases (see Figure 5(a)), variable σ monitoring the battery SOC and representing the distribution between steering and yaw moment generation differs greatly, as depicted in Figure 5(b). Hence, since the battery SOC is assumed to drop below 80 percent at the beginning of the simulation (see Figure 8(c)), the high-level controller is reconfigured with changing the value of σ into zero as the vehicle enters the slope section.

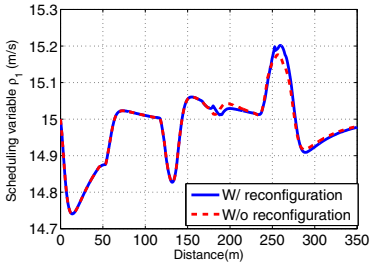

(a) ρ_1

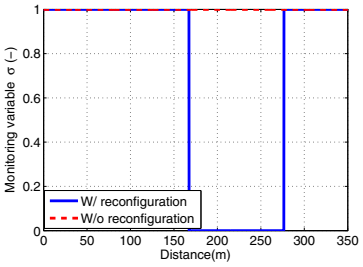

(b) σ

Fig. 5. Scheduling variables of the LPV controller

As the value of σ scales the actuator selection, different high-level control signals are generated in the two cases, see Figure 6. While the longitudinal forces prescribed by the controller are very similar (see Figure 6(a)), the steering angle and yaw moment generation depicted in Figure 6(b) and Figure 6(c) differ greatly at the second corner. It is well demonstrated, that with the battery SOC based reconfiguration method, the steering angle is substituted with yaw moment generation at the second curve, when the vehicle travels on the slope section.

The low-level control signals, i.e the hub motor torques are shown in Figure 7. It can be observed, that compared to the normal case depicted (see Figure 7(a)), with the battery SOC based control reconfiguration significant amount of differential torque is produced with the in-wheel motors (see Figure 7(b)).

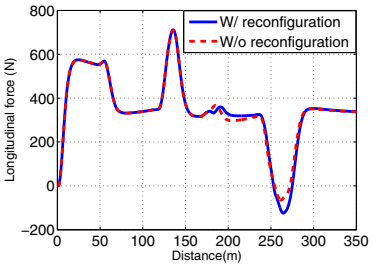

(a) Longitudinal force

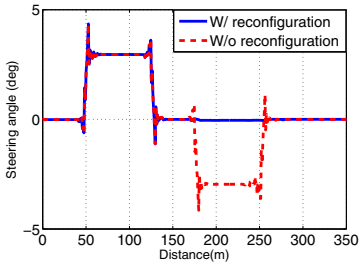

(b) Steering angle

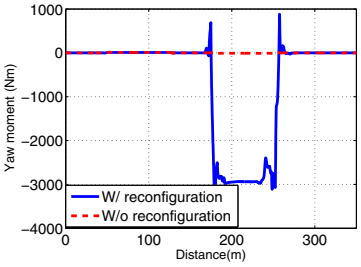

(c) Yaw moment

Fig. 6. High-level control signals

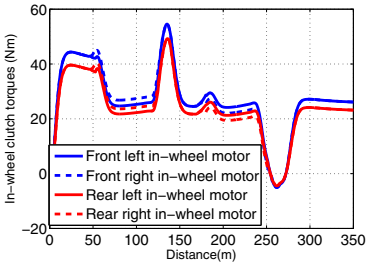

(a) W/o reconfiguration

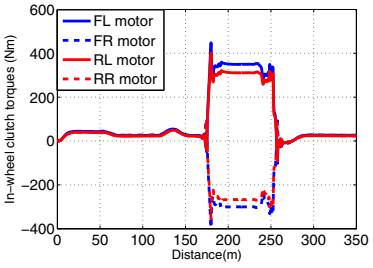

(b) W/ SOC based reconfiguration

Fig. 7. Hub motor clutch torques

The performances of the two different simulations are depicted in Figure 8. Although velocity and yaw rate error shown in Figure 8(a) and Figure 8(b) slightly increased due to the control reconfiguration preferring yaw moment generation over steering intervention, the battery SOC depicted in Figure 8(c) shows the effectiveness of the proposed method. Due to the bigger prescribed negative wheel torques in the second corner on the slope section, bigger amount of recuperation energy could be produced for the battery charging, hence the battery SOC value had bigger value at the end of the simulation.

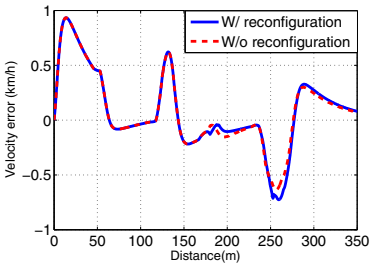

(a) Velocity error

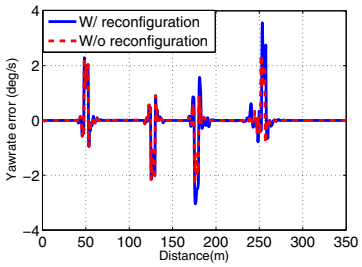

(b) Yawrate error

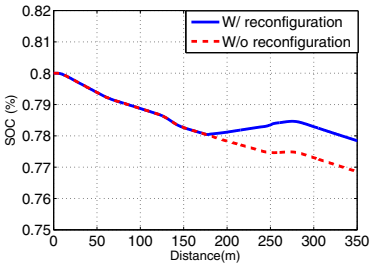

(c) State-of-charge

Fig. 8. Performances of different methods

VI. Conclusion

The paper has introduced a reconfiguration method for 4WIA electric vehicle using hub motors with regenerative braking ability. In case the level of battery SOC is satisfactory, the cornering maneuver of the vehicle is realized with steering. In contrast, if the battery SOC falls below a predefined value and the vehicle is traveling on a slope, the control allocation is altered such way that the cornering maneuver is performed using independent wheel hub torque generation. By this mean, energy recuperation and battery SOC can be enhanced.

References

[1] P. Pudney and P. Howlett, "Critical speed control of a solar car," *Optimization and Enginnering*, vol. 3, pp. 97–107, 2002.

[2] T. A. Ocran, J. Cao, B. Cao, and X. SUN, "Artificial neural network maximum power point tracker for solar electric vehicle," *Tsinghua Science and Technology*, vol. 10, pp. 204–208, 2005.

[3] Z. Shuai, H. Zhang, J. Wang, J. Li, and M. Ouyang, "Lateral motion control for four-wheel-independent-drive electric vehicles using optimal torque allocation and dynamic message priority scheduling," *Control Engineering Practice*, vol. 24, pp. 55–66, 2013.

[4] L. Xiong, Z. Yu, Y. Wang, C. Yang, and Y. Meng, "Vehicle dynamics control of four in-wheel motor drive electric vehicle using gain scheduling based on tyre cornering stiffness estimation," *Vehicle System Dynamics*, vol. 50, pp. 831–846, 2012.

[5] R. Castro, R. E. Araújo, M. Tanelli, S. M. Savaresi, and D. Freitas, "Torque blending and wheel slip control in evs with in-wheel motors," *Vehicle System Dynamics*, vol. 50, pp. 71–94, 2012.

[6] C. L. Cheng and Z. Xu, "Wheel torque distribution of four-wheel-drive electric vehicles based on multi-objective optimization," *Energies 2015*, vol. 8, pp. 3815–3831, 2015.

[7] R. Wang, Y. Chen, D. Feng, X. Huang, and J. Wang, "Development and performance characterization of an electric ground vehicle with independently actuated in-wheel motors," *Journal of Power Sources*, vol. 196, pp. 3962–3971, 2011.

[8] B. Wang, X. Huang, J. Wang, X. Guo, and X. Zhu, "A robust wheel slip ratio control design combining hydraulic and regenerative braking systems for in-wheel-motors-driven electric vehicles," *Journal of the Franklin Institute*, vol. 50, pp. 71–94, 2014.

[9] M. Ringdorfer and M. Horn, "Development of a wheel slip actuator controller for electric vehicles using energy recuperation and hydraulic brake control," *IEEE International Conference on Control Applications, Denver, USA*, pp. 313–318, 2011.

[10] S. Anwar, "Yaw stability control of an automotive vehicle via generalized predictive algorithm," *American Control Conference*, 2005.

[11] Y. Shibahata, K. Shimada, and T. Tomari, "Improvement of vehicle maneuverability by direct yaw moment control," *Vehicle System Dynamics*, 1993.

[12] H. Jing, R. Wang, M. Chadli, C. Hu, F. Yan, and C. Li, "Fault-tolerant control of four-wheel independently actuated electric vehicles with active steering systems," *9th IFAC Symp. Fault Detection, Supervision and Safety for Technical Processes*, vol. 48, pp. 1165–1172, 2015.

[13] R. Rajamani, *Vehicle Dynamics and Control*. Springer, 2005.

[14] J. Bokor and G. Balas, "Linear parameter varying systems: A geometric theory and applications," *16th IFAC World Congress, Prague*, 2005.

[15] F. Wu, X. H. Yang, A. Packard, and G. Becker, "Induced l^2-norm control for LPV systems with bounded parameter variation rates," *International Journal of Nonlinear and Robust Control*, vol. 6, pp. 983–998, 1996.

[16] O. Barbarisi, F. Vasca, and L. Glielmo, "State of charge kalman filter estimator for automotive batteries," *Control Enginnering Practice*, vol. 14, pp. 264–275, 2006.

[17] E. T. M. Verbrugge, "Adaptive state of charge algorithm for nickel metal hydride including hysteresis phenomena," *Journal of Power Sources*, vol. 126, pp. 236–249, 2004.

[18] M. Sorrentino, G. Rizzo, and F. Vasca, "An energetic comparison for hybrid vehicles ranging from low to high degree of hybridization," *10th International Conference on Engines & Vehicles, Capri*, 2011.

[19] P. Lingman and B. Schmidtbauer, "Road slope and vehicle mass estimation using kalman filtering," *Vehicle System Dynamics*, vol. 37, pp. 12–23, 2002.

[20] H. Ohnishi, J. Ishii, M. Kayano, and H. Katayama, "A study on road slope estimation for automatic transmission control," vol. 21, pp. 235–240, 2000.

[21] P. Gáspár, J. Bokor, A. Mihály, Z. Szabó, T. Fülep, and F. Szauter, "Robust reconfigurable control for in-wheel electric vehicles," *9th IFAC Symposium on Fault Detection, Supervision and Safety for Technical Processes (SAFEPROCESS'15)*, pp. 36–41, 2015.

[22] F. Takanori, M. Shogo, M. Kenji, A. Norihiko, and O. Koichi, "Active steering systems based on model reference adaptive nonlinear control," *Vehicle System Dynamics: International Journal of Vehicle Mechanics and Mobility*, vol. 42, pp. 301–318, 2004.

[23] F. Tahami, R. Kazemi, and S. Farhanghi, "A novel driver assist stability system for all-wheel-drive electric vehicles," *IEEE Transactions on Vehicular Technology*, vol. 52, pp. 683–692, 2003.